



# A modified thin-walled tube push-bending process with polyurethane mandrel

Weihao Jiang<sup>1,2</sup> · Wenlong Xie<sup>1,2</sup> · Hongwu Song<sup>1</sup> · Lucian Lazarescu<sup>3</sup> · Shihong Zhang<sup>1</sup> · Dorel Banabic<sup>3</sup>

Received: 5 September 2019 / Accepted: 10 December 2019 / Published online: 21 December 2019  
© Springer-Verlag London Ltd., part of Springer Nature 2019

## Abstract

Thin-walled ( $D/t > 30$ ;  $D$ , initial outer diameter;  $t$ , initial wall thickness) bent tubes with large diameter ( $D > 100$  mm) and small bending radius ( $R/D < 3$ ;  $R$ , centerline radius) are difficult to form integrally using traditional bending methods. In this paper, using a novel loading method, a modified push-bending (MPB) process with polyurethane as mandrel was developed. A stainless steel bent tube with extreme geometrical specification ( $D = 144$  mm,  $D/t = 72$ , and  $R/D = 1.94$ ) was formed integrally by MPB. Based on analytical and finite element (FE) method, the internal pressure, i.e., contact pressure between polyurethane and tube (CPPT) were investigated. The results show that the CPPT decreases linearly from the back end to the front end of polyurethane rod and increases with smaller  $\mu_1$  (the coefficient of friction between polyurethane and tube) and larger  $L$  (the center axis length of polyurethane rod), and the increase of CPPT is helpful to decrease the ovality of the bent tube.

**Keywords** Thin-walled tube · Push-bending · Internal pressure · Polyurethane · Finite element method

## Nomenclature

$D$	initial outer diameter of tube
$t$	initial wall thickness of tube
$R$	centerline radius of bent tube
$\mu_1$	coefficient of friction between polyurethane and tube
$\mu_2$	coefficient of friction between die and tube
$L$	center axis length of polyurethane rod
$dF_{xi}$	tangent compressive resultant force
$dF_{xm}$	tangent force due to the bending moment
$df_i$	friction force between polyurethane mandrel and tube
$df_0$	friction force between die and tube

$dF_{xf}$	tangent force due to the dragging of the stopper
$P_{cx}$	CPPT on certain position
$P'_{cx}$	contact pressure between tube and die on certain position
$E$	elastic modulus
$E_s, \nu$	compression modulus and Poisson's ratio
$\sigma_z, \sigma_\rho, \sigma_\varphi$	axial stress, radial stress, and circumferential stress
$\varepsilon_z, \varepsilon_\rho, \varepsilon_\varphi$	axial strain, radial strain, and circumferential strain
$\theta$	volumetric strain
$K_1, K_2$	constants applied in theoretical analysis
$P_{ax}$	mean axial stress on certain cross-section
$P_{c0}$	CPPT on the cross-section of the back end of the polyurethane mandrel
$F$	pushing force of punch
$F_x$	total axial force on any cross-section of polyurethane mandrel
$S$	cross-sectional area of polyurethane mandrel
$C$	cross-sectional circumference of polyurethane mandrel
$r$	radius of the cross-section of the polyurethane mandrel
$x$	axial distance from the rear end of the polyurethane mandrel

✉ Hongwu Song  
hwsong@imr.ac.cn

<sup>1</sup> Institute of Metal Research, Chinese Academy of Sciences, Shenyang 110016, China

<sup>2</sup> School of Materials Science and Engineering, University of Science and Technology of China, Shenyang 110016, China

<sup>3</sup> Department of Manufacturing Engineering, Technical University of Cluj-Napoca, 400641 Cluj-Napoca, Romania

## 1 Introduction

Thin-walled bent tube components have been extensively used in aviation, aerospace, automobile, oil, and ship industries due to their hollow structure and satisfactory high strength/weight ratio [1–3]. The integral forming of bent tube with extreme geometrical specification ( $D > 100$  mm,  $D/t > 30$ , and  $R/D < 3$ ;  $D$ , initial outer diameter,  $t$ , the initial wall thickness;  $R$ , centerline radius) is hard to be realized [4]. The main defects in the thin-walled tube bending with large diameter include wrinkling, over thinning, and cross-section distortion [5–7].

For thin-walled tube bending with large diameter, various mandrels or fillers were filled into the tube to reduce or avoid these defects. Mandrels in tube bending include rigid mandrels and flexible mandrels [4, 8–10]. Fillers in tube bending include solid particles [11, 12], liquids [13–15] and so on. Because elastomers can be successfully reused multiple times, they are used as a pressure-transmitting medium for various metal-forming operations [16, 17]. During tube push-bending, the elastic mandrel can avoid wrinkling and distortion due to its excellent anti-compression properties. Bello et al. have pioneered elastomer forming technique into tube bending and analyzed experimentally this new tube bending method [18]. Since then, great efforts have been done to research elastomer media-based tube bending. The bending loads supplied in tube bending using elastomer rod as mandrel were estimated by the upper bound theory, which had a good agreement with the experimental results [19]. LF2 aluminum alloy

bent tubes with a bending radius that is equal to the tube diameter were formed successfully by the push-bending method with elastic material as mandrel [20]. A tube bending method with urethane rod as mandrel was developed based on FE simulation, and two different strain energy potential functions used to model urethane were compared [21]. A push-bending process with rubber as mandrel was used to form a stainless steel 304 (SS304) and brass bent tube, and the wrinkling was predicted based on artificial neural network models [22]. Imitating the structure of a *Squilla*, an elastomer mandrel was introduced to NC bending for large diameter-to-thickness ratio thin-walled tubes [23]. A push-bending method using sectional elastomers as mandrel was proposed to form the 5A02 thin-walled aluminum alloy tube with 1D bending radius, 40 mm outer diameter, 1 mm wall thickness, and 90° bending angle [24].

Based on experimental, analytical, or FE method, a lot of studies about elastomer media-based tube bending have been done. However, thin-walled tube bending with large diameter and small bending radius has been scant. In this paper, a modified push-bending process (MPB) with polyurethane as mandrel was developed, and its characteristics were analyzed. A 3D elastic–plastic FE model of the push-bending was set up based on the FE code ABAQUS/Explicit and validated experimentally. Afterwards, based on FE analysis and mathematical derivation, the distribution rules and influence factors of contact pressure between polyurethane and tube (CPPT) were investigated.

**Fig. 1** Schematics of MPB with polyurethane as mandrel. **a** Sectional view along bending plane before bending. **b** Sectional view along bending plane after bending

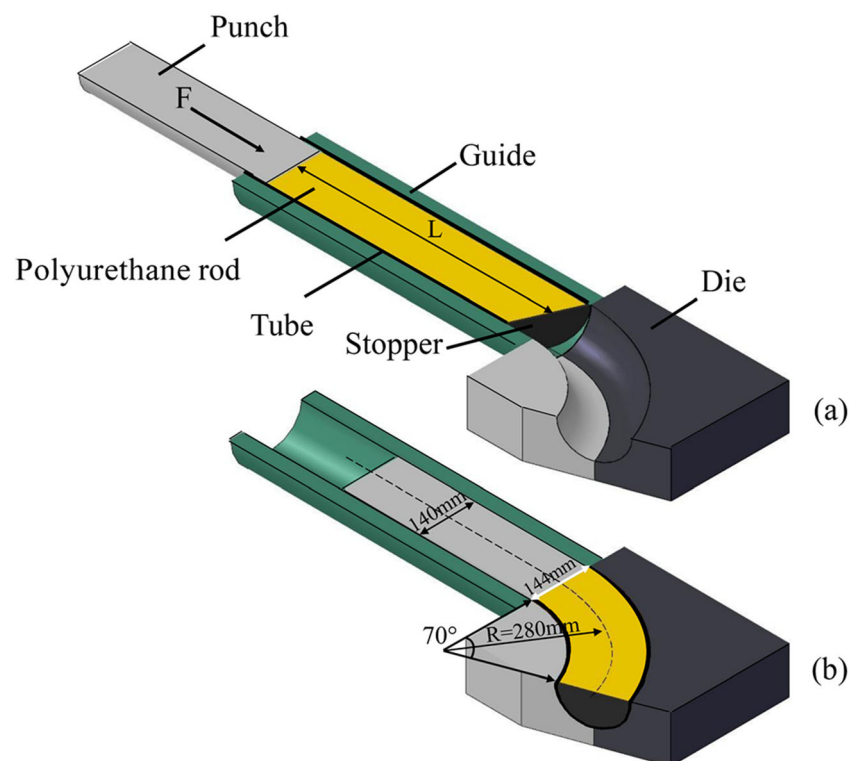
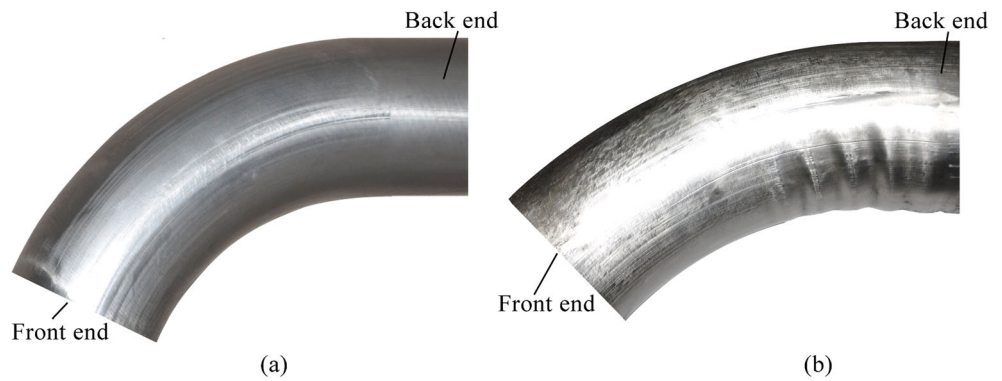


**Fig. 2** Bent tubes obtained from two different loading methods based on push-bending. **a** Without wrinkling when pushing force exerting on only polyurethane mandrel. **b** Wrinkling when pushing force exerting on both back end of tube and polyurethane mandrel



## 2 MPB with polyurethane as mandrel

### 2.1 Principle of MPB

The schematics of MPB with polyurethane as mandrel are illustrated in Fig. 1. Before tube bending, a metal thick sheet is welded on the front end of the tube blank. Then, a polyurethane rod was placed into the tube cavity. Finally, the tube/polyurethane rod assembly in the guide sleeve was placed. During bending, axial pushing force of the punch only imposes on the back end of polyurethane rod. Under the jointly constraining of polyurethane rod and die, the straight tube is formed into a bent one with desired shape. The polyurethane rod promptly recovers its original shape after removing from bent tube, so the same process can be repeated for many times.

### 2.2 Characteristics of MPB

For traditional push-bending methods, the axial pushing force of the punch is imposed on the back end of the tube blank, which will increase the risk of wrinkling due to the increase of tangent compression stress on the inner bending arc. Therefore, the thin-walled tubes with large diameter and small bending radius are hard to form using traditional push-

bending methods. For MPB with polyurethane as mandrel, the pushing force is imposed on the back end of the polyurethane mandrel rather than the tube. Bent tubes formed by two different loading methods based on push-bending process are shown in Fig. 2. It can be seen from Fig. 2 that using MPB with polyurethane as mandrel can effectively restrain the wrinkling of the bent tube.

As shown in Fig. 3, the tangent compressive resultant force exerted on a tiny element of the inner wall of the bent tube can be expressed as:

$$dF_{xi} = dF_{xm} + df_i - df_o - dF_{xf} \tag{1}$$

where  $dF_{xm}$  is the tangent force due to the bending moment,  $dF_{xf}$  is the tangent force due to the dragging of the stopper,  $df_i$  is the friction force between polyurethane mandrel and tube; it can also be expressed as:

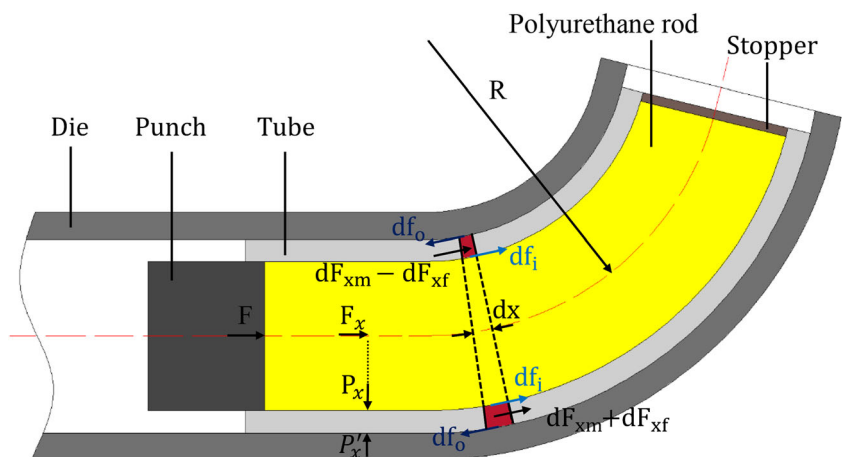
$$df_i = \mu_1 P_{cx} dx \tag{2}$$

where  $P_{cx}$  is the CPPT on certain position,  $df_o$  is the friction force between die and tube; it can also be expressed as:

$$df_o = \mu_2 P'_{cx} dx \tag{3}$$

where  $P'_{cx}$  is the contact pressure between tiny tube element and die on certain position.

**Fig. 3** Force analysis for the bent tube during MPB with polyurethane as mandrel



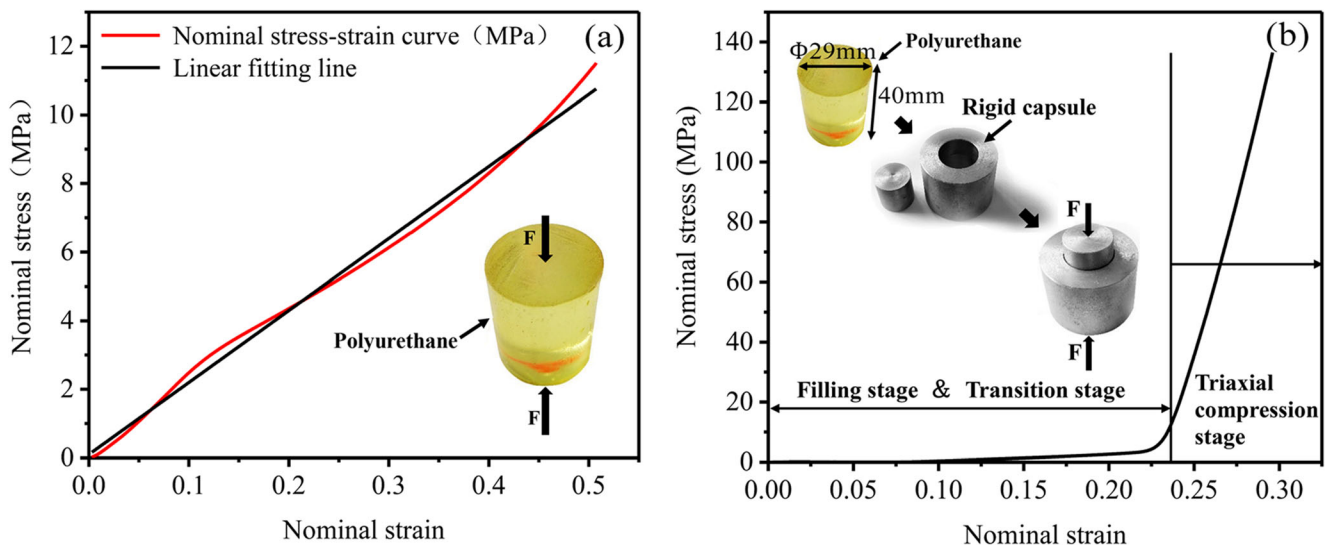


**Fig. 4** Nominal stress-strain curve of polyurethane. **a** Uniaxial compression. **b** Triaxial compression

As shown in Fig. 3 and Eq. (1), axial pushing force  $F$  is transmitted to the stopper through the polyurethane rod to produce a tangent tensile force  $dF_{xf}$  at the tiny tube element to offset a portion of the tangent compressive stress  $dF_{xm}$ , which can decrease  $dF_{xi}$  and reduce the risk of wrinkling.

### 3 FE simulations of the MPB

#### 3.1 Mechanical properties test of polyurethane

Polyurethane is a kind of polymer material with high flexibility and resilience. The Shore A hardness of polyurethane used in this test is 85. A uniaxial compression test and triaxial compression test were carried out on polyurethane with WDW-100kN electronic universal tester. For uniaxial compression test, the compression speed is 5 mm/min, and the compression rate is 50%. For the triaxial compression test, due to the constraints of a rigid capsule, polyurethane is subjected to three-dimensional compressive stress during the

compression. The compression rate is 30%, and the compression speed is 5 mm/min.

As shown in the uniaxial compression nominal stress-strain curve of polyurethane in Fig. 4a, the elastic modulus of polyurethane is very low. The linear fitting of the uniaxial compression nominal stress-strain curve of polyurethane has a slope of 21, i.e., the elastic modulus  $E$  of polyurethane used in the test is 21 MPa. The polyurethane can be totally bounced back to its original state after unloading. Therefore, polyurethane mandrel in tube push-bending can be reused many times.

Because there is a gap between polyurethane and rigid capsule in the initial stage as shown in Fig. 4b, the triaxial compression stress-strain curve of polyurethane is divided into three stages. The first stage is the filling stage, which is similar to uniaxial compression; when the transverse expansion of the polyurethane in contact with the rigid capsule inner wall, into the transition stage; at the third stage, the polyurethane fully filled the capsule cavity, and its stress state becomes three-dimensional compressive stress; the stress rises sharply and has a linear relationship

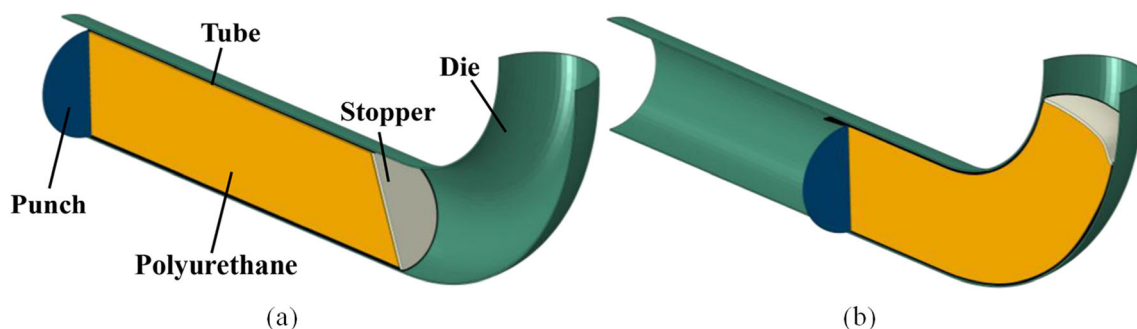


**Fig. 5** Schematics of FE model. **a** Before bending. **b** After bending

**Table 1** Mechanical properties of 0Cr18Ni9 tubular blank at room temperature

Young’s modulus $E$ (MPa)	Density (kg/m <sup>3</sup> )	Elongation (%)	Tensile yield strength (MPa)	Ultimate tension strength (MPa)	Poisson’s ratio
201,000	7930	55	205	620	0.3

with the strain. The slope of the stress-strain curve at the third stage can be calculated as 2088. Therefore, the compression modulus  $E_s$  of the polyurethane used in the test is 2088 MPa.

According to the theory of elastic mechanics, the constitutive equation of the polyurethane rod in the cylindrical coordinate system can be expressed as [25]:

$$\begin{cases} \sigma_z = \frac{E}{1+\nu} \left( \frac{\nu}{1-2\nu} \theta + \varepsilon_z \right) \\ \sigma_\rho = \frac{E}{1+\nu} \left( \frac{\nu}{1-2\nu} \theta + \varepsilon_\rho \right) \\ \sigma_\varphi = \frac{E}{1+\nu} \left( \frac{\nu}{1-2\nu} \theta + \varepsilon_\varphi \right) \end{cases} \quad (4)$$

where,  $\sigma_z$  and  $\varepsilon_z$  are the axial stress and axial strain of the polyurethane rod, respectively;  $\sigma_\rho$  and  $\varepsilon_\rho$  are the radial stress and radial strain of the polyurethane rod, respectively;  $\sigma_\varphi$  and  $\varepsilon_\varphi$  are the circumferential stress and circumferential strain of the polyurethane rod, respectively;  $\nu$  is the Poisson's ratio of polyurethane rod.  $\theta$  is the volumetric strain of the polyurethane rod, and it can be expressed as:

$$\theta = \varepsilon_z + \varepsilon_\rho + \varepsilon_\varphi \quad (5)$$

Since the lateral direction of the polyurethane rod is rigidly fixed  $\varepsilon_\rho = 0$  and  $\varepsilon_\varphi = 0$ , therefore, the  $\varepsilon_z$  in Eq. (4) can be expressed as:

$$\varepsilon_z = \frac{(1+\nu)(1-2\nu)}{1-\nu} \frac{\sigma_z}{E} = \frac{\sigma_z}{E_s} \quad (6)$$

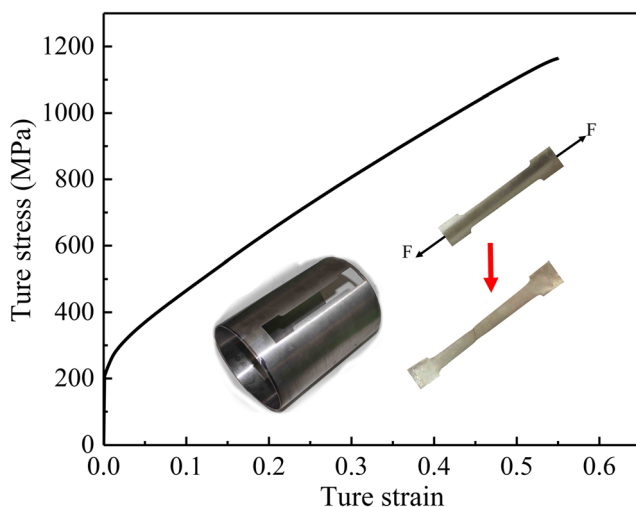


**Fig. 6** True stress-strain curve of 0Cr18Ni9

Equation (6) can be simplified to:

$$E = \frac{(1+\nu)(1-2\nu)}{1-\nu} E_s \quad (7)$$

Therefore, the Poisson's ratio can be derived as:

$$\nu = \frac{\sqrt{(E_s-E)^2 + 8E_s(E_s-E)} - (E_s-E)}{4E_s} \quad (8)$$

Substituting  $E = 21$  MPa and  $E_s = 2088$  MPa into Eq. (8), the result is  $\nu = 0.4983$ . So, the polyurethane in the MPB is weakly compressible materials [26]. Liquids have similar Poisson’s ratio, but sealing problems make them difficult to use in the MPB.

The above results indicate that polyurethane is a typical hyperelastic material, and the above test data can be used in the establishment of the FE model of MPB with polyurethane as mandrel.

### 3.2 Establishment of the FE model

As shown in Fig. 5, a 3D elastic–plastic FE model of MPB with polyurethane as mandrel was established by FE code ABAQUS/Explicit. The dynamic explicit algorithm can simulate large deformation process and complex contact conditions without convergence problem, so it is very suitable to simulate the MPB with polyurethane as mandrel.

The FE model includes the punch, tube, stopper, die (including guide), and polyurethane mandrel. The four-node 3D bilinear quadrilateral rigid element R3D4 was used to model the die and punch. Because the wall thickness of the tube is small relative to the other two directions, tube can be considered to be subject to a plane stress during the bending process. So, the four-node doubly curved thin shell S4R was used to mesh the tube, and 5 integral points was set in the thickness direction of the tube. The material type of the tube is stainless steel 304 (0Cr18Ni9), its mechanical properties at room temperature obtained by tensile test according to EN ISO 6892-1:2009 are presented in Table 1, and the true stress-strain curve at room temperature is shown in Fig. 6. The geometrical dimensions of bent tube are shown in Table 2. The stopper and polyurethane rod were modeled using C3D8R, an eight-node linear brick, reduced integration, hourglass control element.

To describe the behavior of hyperelastic materials, strain energy potential  $U$  is used. There are many options for strain

**Table 2** Basic geometrical dimensions of the bent tube

Initial outer diameter $D$ (mm)	Initial wall thickness $t$ (mm)	Bending radius $R$ (mm)	Bending angle ( $^{\circ}$ )
144	2	280	70

energy potential model in ABAQUS. In this paper, the Marlow strain energy potential model was used to model polyurethane as recommended by Abaqus Analysis User's Guide, i.e., when only one set of test data (uniaxial, equibiaxial, or planar test data) is available, the Marlow form is recommended.

All the friction behavior in the FE model was described by the classic Coulomb friction model  $\tau = \mu P$ , in which the  $\tau$  is the friction shear force,  $\mu$  is the coefficient of friction, and  $P$  is the pressure on the contact surface. A surface-to-surface contact algorithm was employed at the interface between the die and the tube and between the tube and the polyurethane mandrel. Penalty constraints were used to describe the mechanical constraints for the contacts. The coefficients of friction were set according to the references [21–23]. Center axis length of polyurethane rod and coefficients of friction for each simulation are shown in Table 3.

Because of the inherent symmetrical relationship in the actual push-bending, only one-half of the FE model needs to be considered to reduce the computing costs. Proper mass scaling of the model was set to ensure a balance between calculation accuracy and computational efficiency. The limit of mass scaling is to ensure kinetic energy not exceeding 10% of the internal energy.

### 3.3 Experimental validation of the FE model

In order to validate the reliability of the FE model, four sets of experiments with the same conditions were done on the tube bender shown in Fig. 7. The dimensions of tube blank and polyurethane rod used in experiments are the same with the simulation 1 to 4. The contact surface between the tube and

the die was lubricated by the pull stretch oils, and the one between the polyurethane rod and the tube was not lubricated. The forward speed of punch remains in 10 mm/s throughout the tube bending. The bent tubes obtained from experiment and simulation 1 are shown in Fig. 8a and b, respectively.

The wall thickness along the extrados and intrados of the bent tubes obtained from the four sets of experiments was measured by the ultrasonic thickness gauge (Fig. 9), and the measurement positions are shown in Fig. 8a. Average wall thickness of four sets of experiments are shown in Fig. 10a. As shown in Fig. 10b, mean values of pushing force during real tube bending can be obtained directly from the pressure gauge in forming device. Three sets of simulations with different  $\mu_1$  were performed to compare with the experiments. It can be seen in Fig. 10 that the results obtained by FE simulations have a good agreement with the ones obtained from the experiments. Therefore, the FE model is reliable.

## 4 Distribution rules and influence factors of CPPT

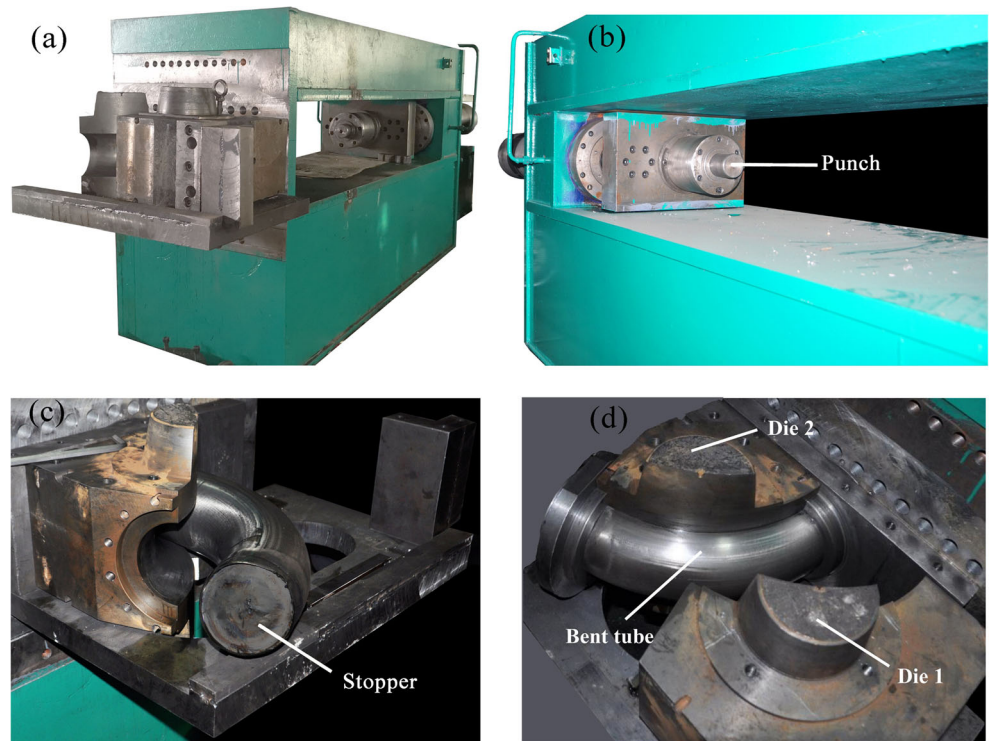
### 4.1 Distribution rules of CPPT

As shown in Fig. 11, a simulation for triaxial compression of a polyurethane rod ( $\phi 139 \times 470$ mm) was conducted by ABAQUS/Explicit. The coefficient of friction between the polyurethane rod and the rigid capsule was 0.1, and the compression displacement was 15 mm. During triaxial compression, the transverse expansion of the polyurethane rod produces a contact pressure on rigid capsule. It can be obviously seen from Fig. 11 that the axial stress and contact pressure

**Table 3** Center axis length of polyurethane rod and coefficient of friction for each simulation

Simulation	Center axis length of polyurethane rod $L$ (mm)	Coefficient of friction between polyurethane and tube $\mu_1$	Coefficient of friction between die and tube $\mu_2$
1	565	0.08	0.1
2	565	0.10	0.1
3	565	0.12	0.1
4	565	0.14	0.1
5	515	0.08	0.1
6	465	0.08	0.1
7	415	0.08	0.1

**Fig. 7** Devices used in tube push-bending experiment. **a** Tube bender. **b** Punch. **c** Stopper. **d** Bent tube and die



between polyurethane and rigid capsule decrease gradually along the direction of axial force  $F$ . Figure 12 is a plot of contact pressure between polyurethane and rigid capsule on certain cross-section vs corresponding mean axial stress. In Fig. 12, the continuous line is extracted from the upper end to the lower end in Fig. 11, and the dotted line is the extension of the continuous line. Linear relationship can be found between the contact pressure and mean axial stress on certain cross-section. Therefore, the contact pressure between polyurethane and rigid capsule on certain cross-section can be expressed as:

$$P_{cx} = K_1 P_{ax} \tag{9}$$

where  $K_1$  is the slope of the line in Fig. 12 and  $P_{ax}$  is mean axial stress on a certain cross-section.

During the tube bending process, the polyurethane rod is subjected to the axial pushing force of the punch. Therefore, the transverse expansion of the polyurethane rod produces a supporting pressure on the tube, so as to avoid wrinkling and cross-section distortion.

Similar to triaxial compression, the CPPT during tube push-bending process is caused by the transverse expansion of polyurethane rod, and the larger the axial stress at the same cross-section of polyurethane rod, the greater the CPPT and vice versa. Since the friction force on the outside surface of polyurethane mandrel partially offsets the axial stress, the

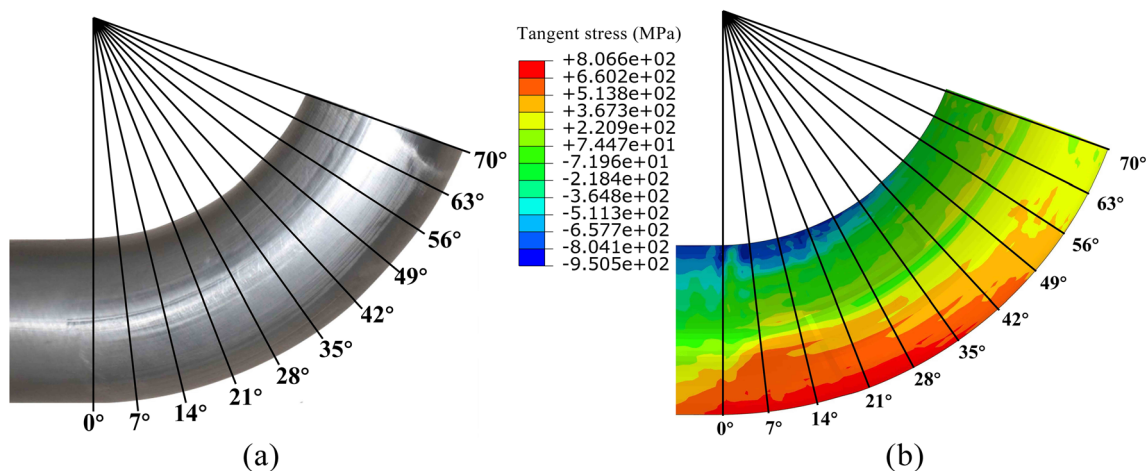


**Fig. 8** The bent tubes obtained from (a) experiment and (b) simulation 1



Fig. 9 Ultrasonic thickness gauge

closer to the front-end of the polyurethane rod, the more the offset is. Therefore, as shown in Fig. 13a, the distribution of CPPT shows a tendency to decrease gradually from the back end to the front end.

As shown in Fig. 13b, the CPPT along the intrados and extrados were extracted to investigate the attenuation law of CPPT. Figure 13b shows that the CPPT decreases linearly within 24~192 mm of straight section and 0~63° of bending section, respectively, but change at the front end due to the rebound tendency of the bent polyurethane rod.

### 4.2 Influence of the Poisson's ratio of polyurethane on CPPT

As mentioned in Section 3.1, the polyurethane used in the MPB with polyurethane as mandrel has a Poisson's ratio ( $\nu$ ) of 0.4983, so it is almost incompressible. It can be seen from

Fig. 14 that a slight decrease in  $\nu$  of the polyurethane can result in significant decrease in CPPT. Therefore, the choice of polyurethane materials is critical for the MPB with polyurethane as mandrel. The greater the  $\nu$ , the higher the CPPT during the tube push-bending, which is beneficial to preventing wrinkling and cross-sectional distortion.

### 4.3 Influence of $\mu_1$ on CPPT

#### 4.3.1 Theoretical analysis

The influence of  $\mu_1$  on CPPT can be theoretically analyzed by the use of the following several assumptions:

- (1) There is the same value of CPPT on the same cross-section of polyurethane mandrel, and Eq. (9) is still available to MPB with polyurethane as mandrel.
- (2) CPPT decreases linearly from the back end to the front end of polyurethane mandrel, and the attenuation gradient is independent of  $\mu_1$ .
- (3) The friction force between tube polyurethane mandrel gradually offset the axial force of the polyurethane mandrel.

According to assumption (1), mean axial stress on certain cross-section  $P_{ax}$  is given by:

$$P_{ax} = \frac{P_{cx}}{K_1} \tag{10}$$

According to assumption (2), CPPT at any cross-section can be expressed as:

$$P_{cx} = P_{c0} - K_2x \tag{11}$$

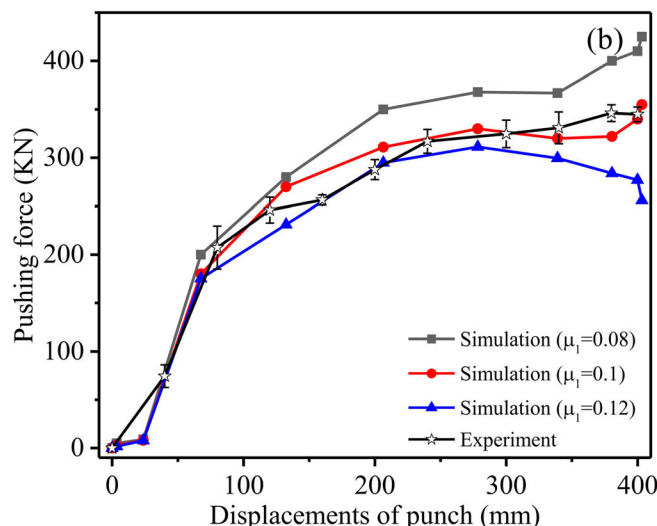
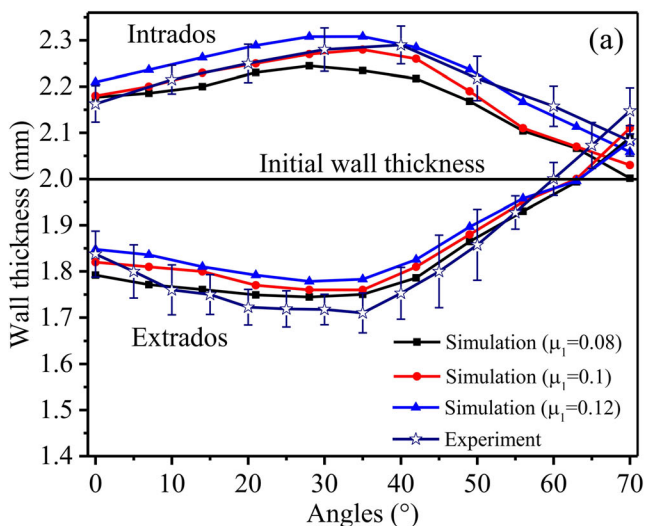
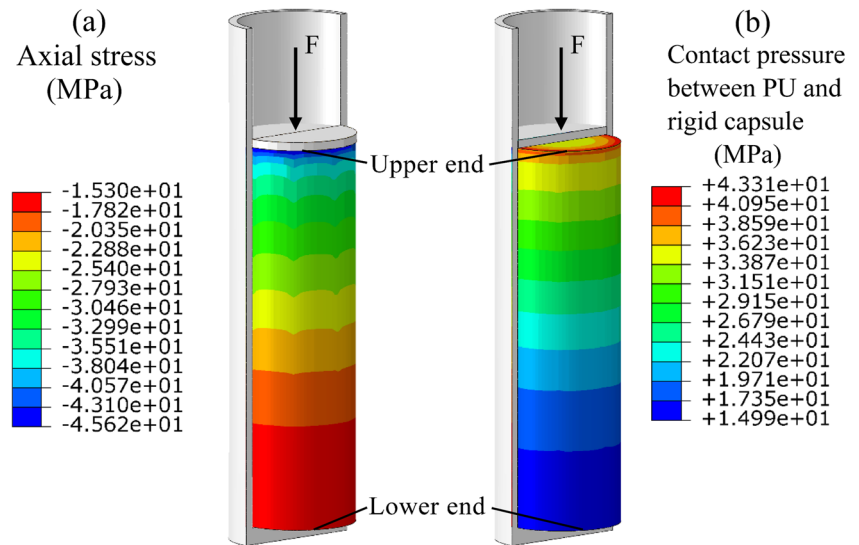


Fig. 10 Results obtained from experiments and simulations. a Wall thickness distributions of tubes. b Pushing force versus displacement of punch



**Fig. 11** Contours of polyurethane during triaxial compression. **a** Axial stress. **b** Contact pressure between polyurethane and rigid capsule



where  $P_{c0}$  is the CPPT on the cross-section of the back end of the polyurethane mandrel and  $K_2$  is a constant. Substituting Eq. (11) into Eq. (10), then Eq. (10) becomes:

$$P_{ax} = P_{a0} - \frac{K_2}{K_1}x \tag{12}$$

Obviously, total axial force on any cross-section of polyurethane mandrel can be expressed as:

$$F_x = SP_{ax} = SP_{a0} - \frac{SK_2}{K_1}x = F - \frac{SK_2}{K_1}x \tag{13}$$

where  $S$  is the cross-sectional area of the polyurethane mandrel and  $F$  is the pushing force applied on the back end of the

polyurethane mandrel. According to assumption (3), total axial force on any cross-section can be expressed as:

$$F_x = F - \int_0^x \mu_1 P_{cx} C dx \tag{14}$$

where  $C$  is the cross-sectional circumference of polyurethane mandrel. Comparing the Eq. (13) and Eq. (14), then:

$$\frac{SK_2}{K_1}x = \int_0^x \mu_1 P_{cx} C dx \tag{15}$$

Substituting Eq. (11) into Eq. (15), then:

$$\frac{SK_2}{K_1} = \mu_1 C (P_{cx} + 0.5K_2x) \tag{16}$$

Hence, when the pushing force of punch is a constant, the relationship between  $P_{cx}$  and  $\mu_1$  can be expressed as:

$$P_{cx} = \frac{SK_2}{CK_1\mu_1} - 0.5K_2x = \frac{rK_2}{2K_1\mu_1} - 0.5K_2x \tag{17}$$

where  $r$  is the radius of the cross section of the polyurethane mandrel. Equation (17) can also be expressed as:

$$P_{cx} = \frac{A}{\mu_1} - Bx \tag{18}$$

where

$$A = \frac{rK_2}{2K_1}$$

and

$$B = 0.5K_2$$

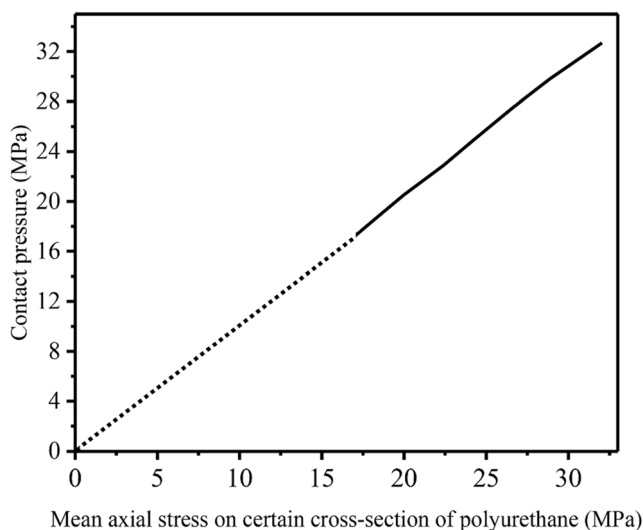


**Fig. 12** Contact pressure between polyurethane and rigid capsule on certain cross-section versus corresponding mean axial stress during triaxial compression

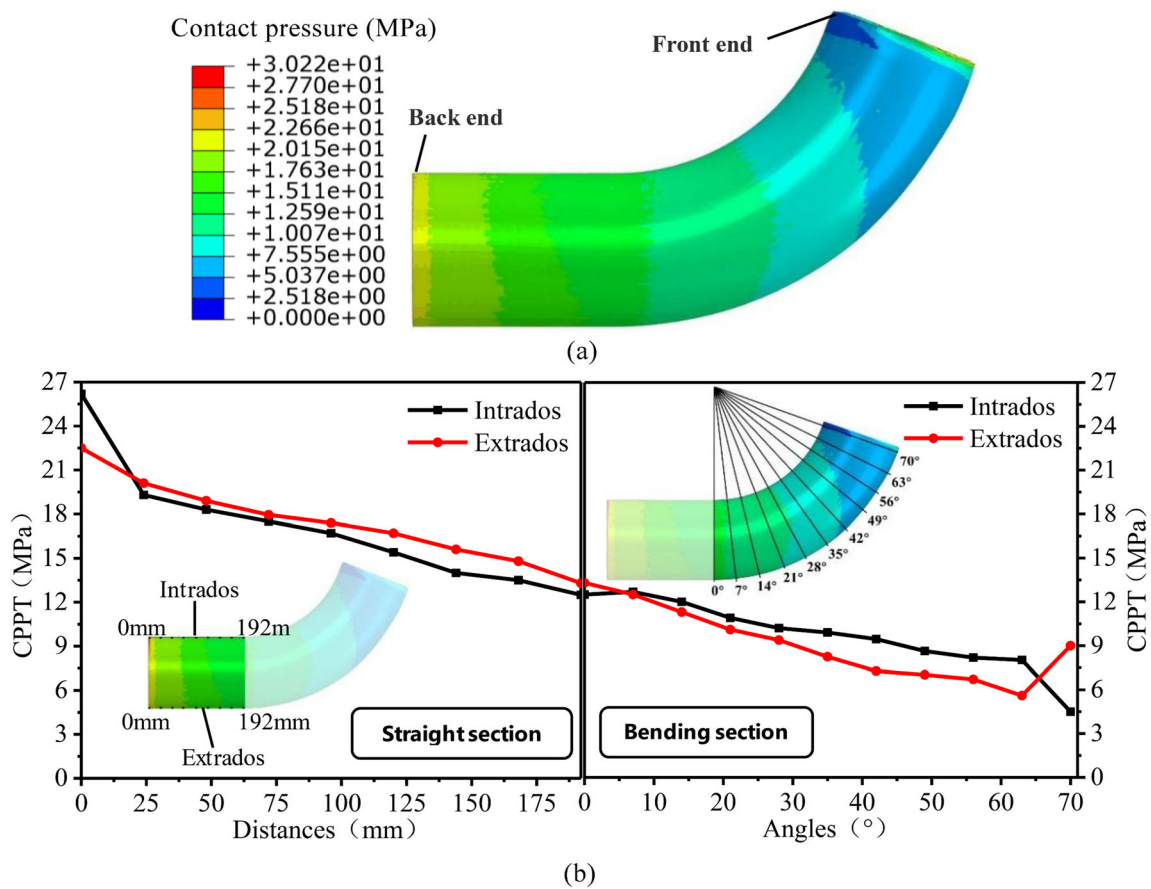


Fig. 13 Distribution of CPPT when  $\mu = 0.1$ . a Contour plot of CPPT. b Variation curves of CPPT along intrados and extrados

In this paper,  $A$  and  $B$  are constants. Equation (18) shows that  $P_{cx}$  on certain position ( $x$  is constant) decreases with the increase of  $\mu_1$ , which causes the decrease of total friction force between the tube and the die. Therefore, the pushing force of the punch required during tube bending will reduce, which causes the further reducing of the CPPT.

### 4.3.2 FE analysis

To validate the above theoretical analyses, as shown in Fig. 15, CPPT along the extrados with different  $\mu_1$  values were extracted. It can be seen from Fig. 15 that under different  $\mu_1$  values, CPPT is almost linearly reduced from the back to the

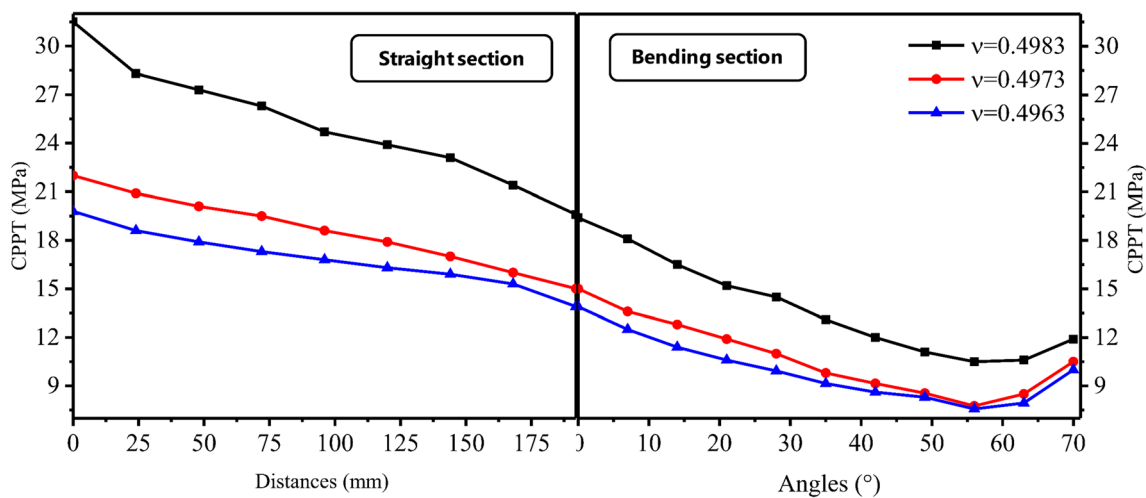


Fig. 14 Variation curves of CPPT along extrados under different Poisson's ratio ( $\nu$ ) of polyurethane

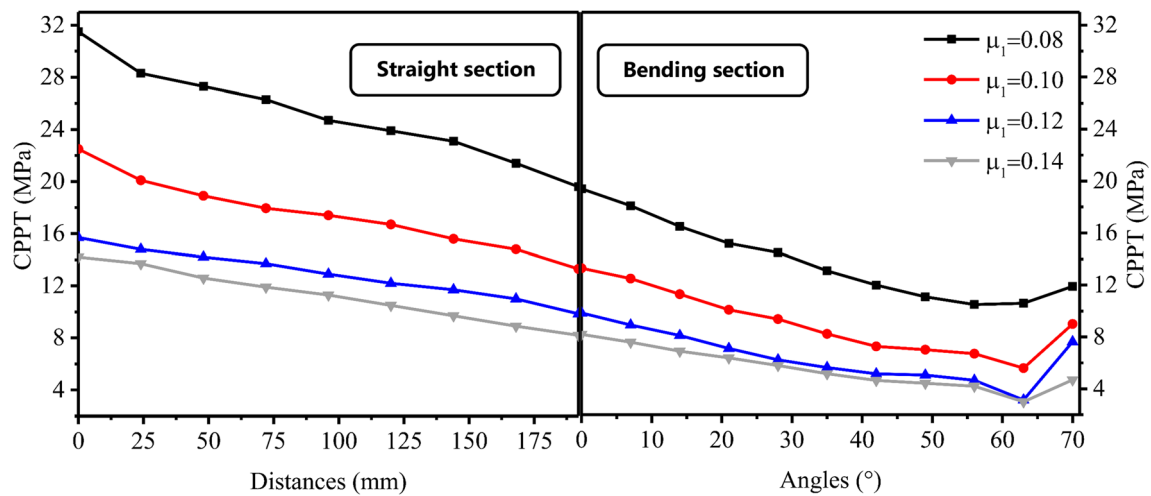


Fig. 15 Distributions of CPPT along extrados of bending section under different

front, and the reduction gradient changes a little with the change of CPPT.  $K_1$  is the slope of the line in Fig. 12, so  $K_1 = 1.03$  can be obtained by linear fitting. Data of the straight section in Fig. 15 was linearly fitted to obtain slopes of 0.05, 0.04, 0.03, and 0.03, respectively. Their average is 0.0375, so  $K_2 = 0.0375$ . Since the radius of the cross-section of the polyurethane mandrel used in this paper is 69.5 mm, therefore  $A = 1.27$  and  $B = 0.02$ . Equation (18) can also be expressed as:

$$P_{cx} = \frac{127}{100\mu_1} - 0.02x \tag{19}$$

when  $x = 120$  mm, the analytical results and simulation results of the relationship between CPPT and  $\mu_1$  are shown in Fig. 16. As can be seen from Fig. 16, there is error between the theoretical analytical results and the simulation results, but the effect of  $\mu_1$  on CPPT is the same. The error between them is mainly caused by various basic assumptions.

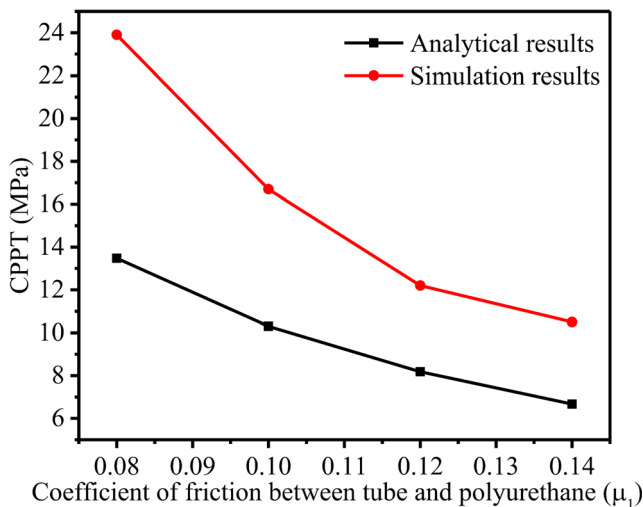


Fig. 16 Analytical results and simulation results of the relationship between CPPT and ( $x = 120$  mm)

During the tube bending, the outer wall of the bent tube tends to collapse if the internal support is insufficient, which causes the cross-section to be ovalized. In order to assess the flattening of cross-section, the maximum cross-section ovality is defined as:

$$\varphi = \frac{D - D_{\min}}{D} \tag{20}$$

where  $D$  is the initial tube outer diameter,  $D_{\min}$  is the minimum tube outer diameter after bending. It can be seen from Fig. 17 that increasing  $\mu_1$  will cause a significant increase in maximum cross-section ovality. The reason is that the increase of  $\mu_1$  leads to the decrease of CPPT, which causes insufficient support force in the tube. Therefore, the larger the CPPT, the smaller the cross-sectional distortion.

Therefore, the lubrication between polyurethane mandrel and tube is critical. In actual production, the reasonable

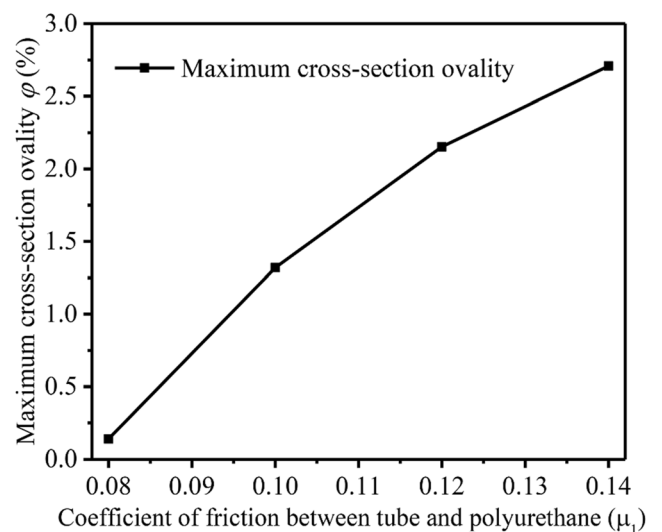
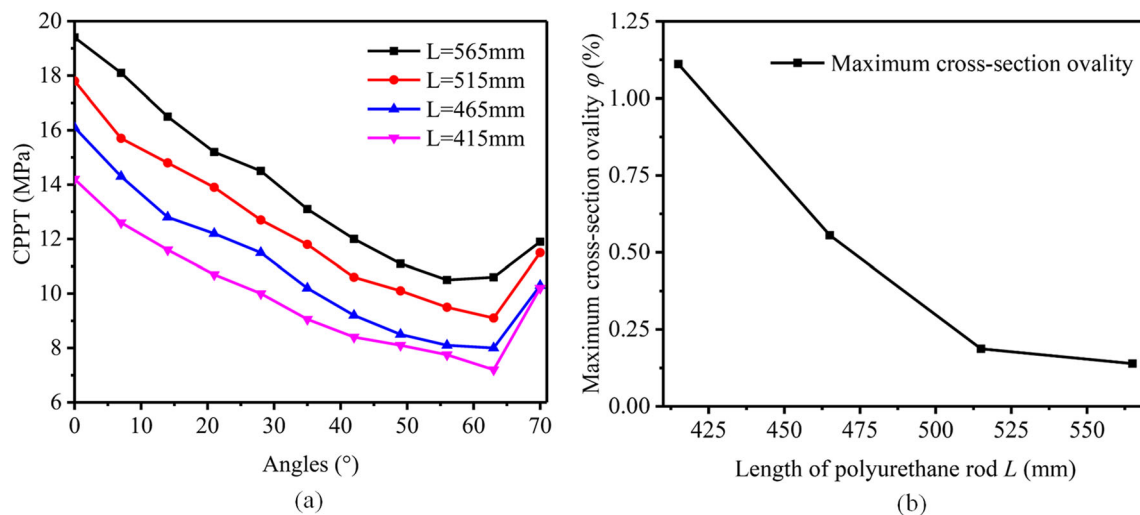


Fig. 17 Influence of on the maximum cross-section ovality



**Fig. 18** **a** Distribution curves of CPPT on bending section of the polyurethane rod under different  $L$ . **b** Influence of  $L$  on maximum cross-section ovality

lubrication method is appropriately decreasing  $\mu_1$  to decrease cross-section distortion.

#### 4.4 Influence of $L$ on CPPT

In order to investigate the influence of  $L$  on the CPPT of bending section, the distributions of CPPT in simulation 1, 5, 6, and 7 are compared in Fig. 18a. It can be found that reducing  $L$  will decrease the CPPT of the bending section.

In Fig. 18b, it is shown that  $L$  has a significant influence on cross-section ovality of bent tube. As the  $L$  increases from 415 to 515 mm, the maximum cross-section ovality significantly decreases, and when  $L$  increases from 515 to 565 mm, the maximum cross-section ovality slightly decreases. Therefore, the value of  $L$  is another critical factor for the MPB with polyurethane as mandrel. In actual production, in order to reduce the cross-section ovality of the bent tube,  $L$  can be appropriately increased, but the excessive  $L$  value cannot effectively decrease the cross-section ovality and increase the cutting loss.

## 5 Conclusions

A MPB with polyurethane as mandrel was developed for thin-walled bent tube with large diameter and small bending radius. The FE model of MPB with polyurethane as mandrel was established, and wall thickness of bent tube and pushing force during bending process in FE simulation and experiment were compared to validate the reliability of FE model. Based on the analytical method and FE analysis, the distribution rules and influence factors of CPPT were investigated. The main conclusions obtained are as follows:

- (1) A bent tube with extreme geometrical specification ( $t = 2$  mm,  $D = 144$  mm, and  $R = 280$  mm) was successfully formed by MPB with polyurethane as mandrel.
- (2) The CPPT decreases linearly from the back end to the front end of polyurethane rod and increases with smaller  $\mu_1$  and larger  $L$ . The increase of CPPT is helpful to decrease the ovality of bent tube.
- (3) Future work will concentrate on improving the FE models to optimize the MPB with polyurethane as mandrel.

**Funding information** The authors appreciate the support from the National Natural Science Foundation of China, China (Grant No. 51875547).

## References

1. Yang H, Lin Y (2004) Wrinkling analysis for forming limit of tube bending processes. *J Mater Process Technol* 152(3):363–369. <https://doi.org/10.1016/j.jmatprotec.2004.04.410>
2. Yang H, Li H, Zhang ZY, Zhan M, Liu J, Li GJ (2012) Advances and trends on tube bending forming technologies. *Chin J Aeronaut* 25(1):1–12. [https://doi.org/10.1016/S1000-9361\(11\)60356-7](https://doi.org/10.1016/S1000-9361(11)60356-7)
3. Wang X, Cao J (2000) Wrinkling limit in tube bending. *J Eng Mater Technol* 123(4):430–435. <https://doi.org/10.1115/1.1395018>
4. Li H, Yang H, Zhang ZY, Li GJ, Liu N, Welo T (2014) Multiple instability-constrained tube bending limits. *J Mater Process Technol* 214(2):445–455. <https://doi.org/10.1016/j.jmatprotec.2013.09.027>
5. Li H, Yang H, Yan J, Zhan M (2009) Numerical study on deformation behaviors of thin-walled tube NC bending with large diameter and small bending radius. *Comput Mater Sci* 45(4):0–934. <https://doi.org/10.1016/j.commatsci.2008.12.018>
6. Zhang Z, Yang H, Li H, Tao ZJ, Wang D (2014) Thermo-mechanical coupled 3D-FE modeling of heat rotary draw bending for large-diameter thin-walled CP-Ti tube. *Int J Adv Manuf Technol* 72(9–12):1187–1203. <https://doi.org/10.1007/s00170-014-5709-7>
7. Li H, Yang H, Xu J, Liu H, Wang D, Li GJ (2013) Knowledge-based substep deterministic optimization of large diameter thin-

- walled Al-alloy tube bending. *Int J Adv Manuf Technol* 68:1989–2004. <https://doi.org/10.1007/s00170-013-4811-6>
8. Guo XZ, Jie T, Zheng Y (2011) Effects of rigid mandrel and lubrication on the process of elbow parts by cold push-bending. *Adv Sci Lett* 4(8):2618–2622. <https://doi.org/10.1166/asl.2011.1354>
  9. Li H, Yang H, Zhan M, Sun ZC, Gu RJ (2007) Role of mandrel in NC precision bending process of thin-walled tube. *Int J Mach Tool Manu* 47(7–8):1164–1175. <https://doi.org/10.1016/j.ijmactools.2006.09.001>
  10. Yang H, Yan J, Zhan M, Li H, Yi K (2009) 3D numerical study on wrinkling characteristics in NC bending of aluminum alloy thin-walled tubes with large diameters under multi-die constraints. *Comput Mater Sci* 45(4):1052–1067. <https://doi.org/10.1016/j.commatsci.2009.01.010>
  11. Liu H, Zhang SH, Song HW, Shi GL, Cheng M (2019) 3D FEM-DEM coupling analysis for granular-media-based thin-wall elbow tube push-bending process. *Int J Mater Form*. <https://doi.org/10.1007/s12289-019-01473-8>
  12. Liu H, Zhang SH, Cheng M, Song HW, Liu JS (2013) DEM simulation of bead packs as fillers in thin-wall tube push bending process. *Am Inst Phys*. <https://doi.org/10.1063/1.4806899>
  13. Montazeri S, Gorji A, Bakhshi M (2015) A new method for compression bending of thin-walled tubes in hydro-bending process. *Int J Adv Manuf Technol* 85(1–4):557–571. <https://doi.org/10.1007/s00170-015-7910-8>
  14. Xie WC, Teng BG, Yuan SJ (2015) Deformation analysis of hydro-bending of bi-layered metal tubes. *Int J Adv Manuf Technol* 79(1–4):211–219. <https://doi.org/10.1007/s00170-015-6830-y>
  15. Lăzărescu L (2012) Effect of internal fluid pressure on quality of aluminum alloy tube in rotary draw bending. *Int J Adv Manuf Technol* 64(1–4):85–91. <https://doi.org/10.1007/s00170-012-3992-8>
  16. Alqureshi HA (1978) On the mechanics of sheet-metal bending with confined compressible dies. *J Mech Work Technol* 1(3):261–275. [https://doi.org/10.1016/0378-3804\(78\)90030-X](https://doi.org/10.1016/0378-3804(78)90030-X)
  17. Thiruvavurudchelvan S (2002) The potential role of flexible tools in metal forming. *J Mater Process Technol* 122(2):293–300. [https://doi.org/10.1016/S0924-0136\(02\)00077-8](https://doi.org/10.1016/S0924-0136(02)00077-8)
  18. Bello EM, Sorensen SB, Al-Qureshi HA (1988) Fabrication of toroidal vessel section using elastomer mandrel Proceedings of the Twenty-Seventh International Matador Conference. Macmillan Education UK. [https://doi.org/10.1007/978-1-349-09912-2\\_46](https://doi.org/10.1007/978-1-349-09912-2_46)
  19. Al-Qureshi HA (1999) Elastic-plastic analysis of tube bending. *Int J Mach Tool Manu* 39:87–104. [https://doi.org/10.1016/S0890-6955\(98\)00012-1](https://doi.org/10.1016/S0890-6955(98)00012-1)
  20. Zeng YS, Li ZQ (2002) Experimental research on the tube push-bending process. *J Mater Process Technol* 122(2):237–240. [https://doi.org/10.1016/S0924-0136\(02\)00027-4](https://doi.org/10.1016/S0924-0136(02)00027-4)
  21. Baudin S, Ray P, Donald BJM, Hashmi MSJ (2004) Development of a novel method of tube bending using finite element simulation. *J Mater Process Technol* 153–154:128–133. <https://doi.org/10.1016/j.jmatprotec.2004.04.205>
  22. Kami A, Dariani BM (2011) Prediction of wrinkling in thin-walled tube push-bending process using artificial neural network and finite element method. *Proc Inst Mech Eng B J Eng Manuf* 225(10):1801–1812. <https://doi.org/10.1177/0954405411404300>
  23. Jiang LF, Zhang SY, Wang YQ, Feng YX, Lin YC, Liu H, Zhang F, Shao H (2019) Research on bending forming method of large diameter-thickness ratio thin-walled tubes for aerospace. *Int J Adv Manuf Technol* 102(9–12):3037–3049. <https://doi.org/10.1007/s00170-019-03328-7>
  24. Xu XF, Wu KW, Wu YW, Fu CL, Fan YB (2019) Push-bending method development of thin-walled tube with relative bending radius of 1 using sectional elastomers as mandrel. *Int J Adv Manuf Technol* 105:995–1008. <https://doi.org/10.1007/s00170-019-04266-0>
  25. Zhou J, Mei ZY, Wang YL (2018) Test method of Poisson's ratio for low modulus elastomer. *Chin J Ship Res* 13(2):91–96 (in Chinese)
  26. Greaves GN, Greer AL, Lakes RS, Rouxel T (2011) Poisson's ratio and modern materials. *Nat Mater* 10(11):823–837. <https://doi.org/10.1038/nmat3134>

**Publisher's note** Springer Nature remains neutral with regard to jurisdictional claims in published maps and institutional affiliations.